Title
Dynamics of Subnanometer Pt Clusters Can Break the Scaling Relationships in Catalysis

Journal
The Journal of Physical Chemistry Letters, 10(3)

ISSN
1948-7185

Authors
Zandkarimi, Borna
Alexandrova, Anastassia N

Publication Date
2019-02-07

DOI
10.1021/acs.jpclett.8b03680

Peer reviewed

Dynamics of Subnanometer Pt Clusters Can Break the Scaling Relationships in Catalysis

Journal:	*The Journal of Physical Chemistry Letters*
Manuscript ID	jz-2018-03680w.R1
Manuscript Type:	Letter
Date Submitted by the Author:	n/a
Complete List of Authors:	Zandkarimi, Borna; UCLA Division of Physical Sciences, Chemistry & Biochemistry Alexandrova, Anastassia; University of California Los Angeles, Chemistry and Biochemistry

Dynamics of Subnanometer Pt Clusters Can Break the Scaling Relationships in Catalysis

Borna Zandkarimi[†] and Anastassia N. Alexandrova[*,†,‡]

[†]Department of Chemistry and Biochemistry, University of California, Los Angeles, Los Angeles, California 90095, United States

[‡]California NanoSystems Institute, Los Angeles, California 90095, United States

[*]Corresponding author's email: ana@chem.ucla.edu

ABSTRACT Scaling relationships in catalysis impose fundamental limitations on the catalyst maximal performance, and so there is a continuous hunt for ways of circumventing them. We show that, at the subnano-scale, scaling relationships can be broken through catalyst dynamics. Oxygen reduction reaction (ORR), which can be catalyzed by Pt nanoparticles, is used as our study case. Subnanometer gas phase and graphene-deposited Pt_n cluster catalysts are shown to exhibit poor correlation between binding energies of intermediates, O, OH, and OOH, involved in the scaling relationships for ORR. The effect is due to the highly fluxional behavior of subnanometer clusters, which easily adapt their structures to the bound adsorbates and varying coverage, and in some cases even reshaping the structure upon changing environment. This fluxional behavior is also commonplace for clusters, and contrasts them to extended surfaces, suggesting that breaking scaling relationships is likely a rule more than an exception in nanocluster catalysis.

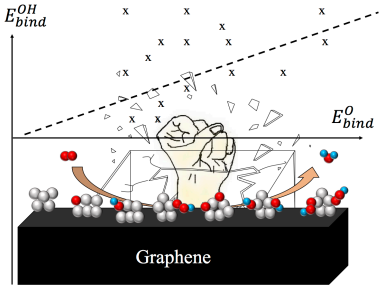

Table of content graphics

Scaling relationships in catalysis provide a simple linear relationship between thermodynamic properties of chemically related species involved in a catalyzed reaction, across a range of catalytic surfaces. Examples include correlations between NH and NH_2 binding energies in ammonia synthesis, and between O, OH, and OOH in the oxygen reduction reaction (ORR). These simple but elegant relations have drawn the attention of many researchers in catalysis.[1–9] Although this simplicity leads to the ability to describe catalytic systems in terms of simple descriptors, such as the position of the d-band center and coordination numbers, scaling relations put an intrinsic limitation on the catalyst maximum activity. In fact, volcano plots are the results of linear relations between the kinetics and thermodynamics of the catalyzed reaction, implying that there is a maximum (at the top of the volcano) for the catalytic activity for each reaction.[1,2,5,10,11] Hence, there has been some efforts to find ways to break the scaling relationships, and thus enhance the catalytic performance beyond the imposed maximum.[12–14] Here, we explore the properties of subnano Pt clusters in the nonscalable regime, i.e. a regime where properties change non-monotonously with changes in cluster size, in the context of ORR catalysis as an example. We show that small Pt clusters do not necessarily follow a highly correlated linear relation and can potentially break the scaling relations, opening opportunities for outstanding catalytic performance.

The mechanism of ORR has been extensively investigated in the past.[15,16,25,17–24] It is known that platinum nanoparticles can catalyze ORR.[26–28] Although nanoparticles with smaller size, around 1 nm, cannot efficiently catalyze ORR due to poisoning,[29] it has been shown that Pt subnano clusters catalyze ORR at even higher rate than nanoparticles.[30–32] Both gas phase and

surface-deposited Pt subnanometer clusters have been studied theoretically and experimentally for the catalysis of ORR.[31,33,34] Since the mechanism of this reaction is the same in the solution and in the gas phase,[35] and the gas phase case is more computationally feasible, gas phase Pt clusters have been more attractive for theoretical studies. Moreover, the approach is justified by the fact that graphene, being a suitable electrode material, causes no significant change to the geometries of the gas phase Pt clusters, such as Pt_{13}, upon deposition.[35] This study considers gas phase and graphene-deposited Pt_n clusters of varying sizes, and addresses the ORR scaling relations in the subnano regime.

For ORR, different mechanisms have been proposed in acidic and alkaline solutions, among which the four-electron process in acidic solution can be written as[36]

$$O_2 + 4H^+ + 4e^- \rightarrow 2H_2O. \quad (1)$$

In the dissociative mechanism of the reaction, O, OH, and OOH are the involved intermediates.[17] These are also the species whose binding energies to the catalysts typically correlate. In this study we show that the correlation between the binding energies of each pair of these molecular fragments to Pt subnano clusters is weak, and the reason is the structural fluxionality of clusters that easily change upon changing adsorbate and coverage. Importantly, this is a test case, while the conclusions are potentially generalizable to other types of subnano clusters and other catalytic processes bound by scaling relations. Cluster dynamics emerges as a potential tool for circumventing scaling relations.

Figure 1 shows the correlation between the calculated OH and O binding energies to the gas phase Pt_n (n=1-6) clusters. The binding energies are calculated for the first adsorbate binding to the cluster, and then also the second adsorbate of the same kind. Cluster geometries with and without bound adsorbates are found through global optimization of structures generated based on the Bond Length Distribution Algorithm (BLDA).[37,38] The geometries are in agreement with the ones obtained from Birmingham Parallel Genetic Algorithm (BPGA).[39] The adsorbate binding energies are calculated with respect to the gas phase adsorbate and (i) the global minimum of the adsorbate-free cluster, or (ii) the global minimum of the cluster with the first adsorbate bound, for the first and second adsorption energy calculations, respectively.

In the lower panel, the blue circles and triangles correspond to the binding energies of the first and second adsorbate, respectively, obtained from DFT calculations using the PBE functional. Since the effective valency changes from 2 for O to 1 for OH, the expected slope of the line that relates their adsorption energies is 0.5. As can be seen, the slope of the line computed for the global minima of subnano clusters is deviated significantly from 0.5. The slope of the line indicates the contribution of the cluster to the optimal electron density of the bound atom, i.e. oxygen, in our case.[1,2] When the slope is significantly less than 0.5, this means that the cluster contributes less than expected to the oxygen electron density. The effect implies that effective medium theorem might not be a good approximation for small clusters. In fact, this is not unexpected since the behavior of small clusters is far from metallic. Additionally, the R^2 of 0.516 shows a poor correlation between data points. Moreover, mean absolute error (MAE) and mean unsigned error (MUE) have been calculated for both first and second binding energies. For PBE calculations, MAEs for all, first, and second binding energies are 0.12 eV, 0.16 eV, and 0.09 eV respectively. Note that mean unsigned errors (MUEs) for the first and second binding energies are -0.01 eV and 0.02 eV respectively and will cancel out each other. The net result is that the predictability of the trend line might not be robust and reliable. The message holds true also for the PBE0 calculations, though in this case, the correlation is even worse (R^2 = 0.204), and the deviation from the expected slope value of 0.5 is also larger (0.335). Furthermore, obtained MAEs for all, first, and second binding energies are 0.19 eV, 0.20 eV, and 0.18 eV respectively. Again because of the different sign of MUE for the first and second binding energy (-0.03 eV and 0.03 eV) they cancel out each other. The binding energies calculated with PBE0 are generally smaller, but the trends in cluster size correlate well with those calculated with PBE. Detailed discussion of the effect of functional on the results can be found in the SI.

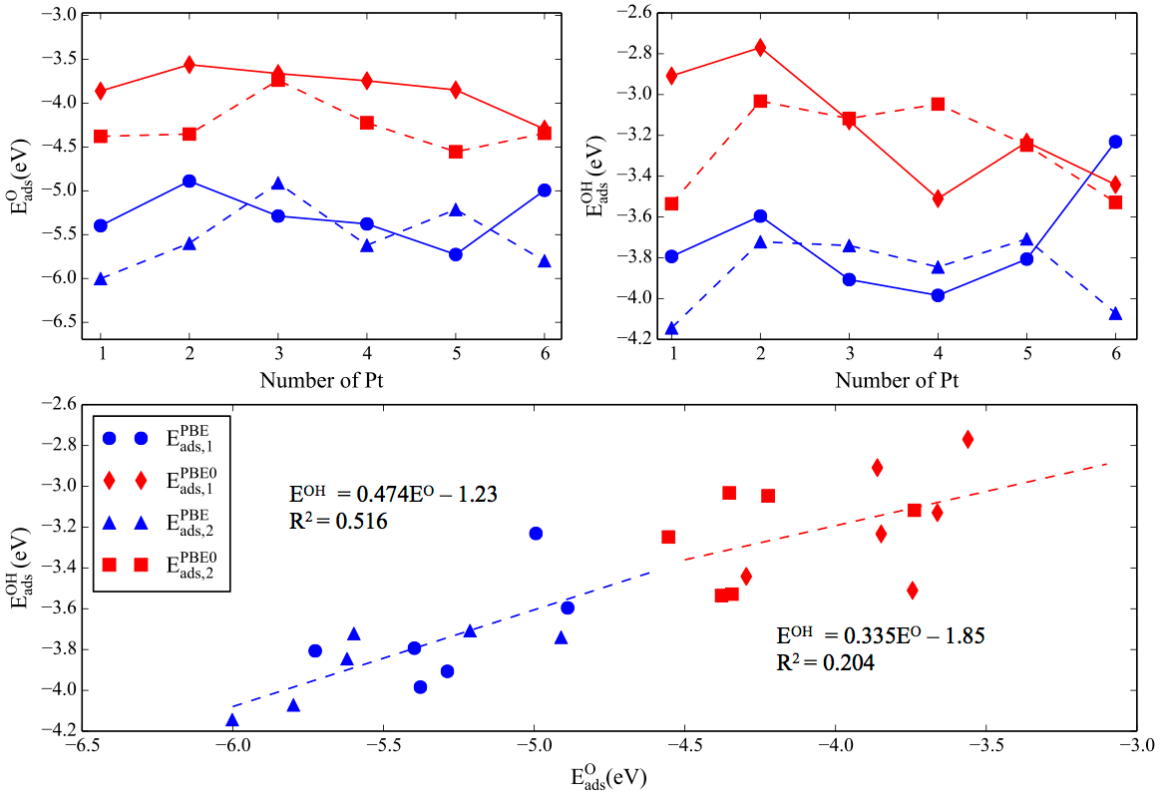

Figure 1. Scaling relationship between OH and O binding energies. The blue and red data sets correspond to the PBE and PBE0 calculations, respectively. Upper panel: the changes in the adsorption energies of O (left) and OH (right) as a function of cluster size; the binding energies of the first adsorbate are connected with the solid line, and the binding energies of the second adsorbate binding to the cluster are connected with a dashed line. Lower panel: correlations of the O and OH binding energies, computed with PBE and PBE0, in blue and red, respectively. Data points represent all studies cluster sizes, and both coverages. The R^2 values showcase the poor correlations. The slope of the line is far from the expected 0.5. Also, MAE for PBE data points is 0.12 eV and for PBE0 data points is 0.19 eV. MUE does not give a meaningful result due to the cancelation of error.

In order to illuminate the found poor correlations, we compare OH and O binding energy trends across the cluster sizes. In the upper panel, first and second binding energies are plotted as a function of number of Pt atoms. It is clear that OH and O binding energies do not have the same trends as a function of cluster size, resulting in the poor correlation. For instance, Pt_5 has the highest O binding energy, whereas Pt_4 has the highest OH binding energy (Figure 1, upper

panel, blue circles connected with the solid line). Furthermore, there is an increase in the O binding energy from Pt_4 to Pt_5. On the other hand, the OH binding energy decreases from Pt_4 to Pt_5. Similar observations can be made for the second adsorbate binding energies (Figure 1, upper panel, blue triangles connected with the dashed line). Interestingly, however, the second adsorbate can bind to the cluster either more or less strongly than the first adsorbate, depending on the cluster size. For example, second O binds to Pt_4 more strongly than the first O, and that is exactly opposite for the OH binding energy (Figure 1, upper panel, blue lines).

The OOH and O binding energies and their correlations are shown in Figure 2. Clearly the correlation is even worse than that in the case of OH and O. The slope of the line obtained from PBE is 0.388 (compare with 0.474 for OH and O), and R^2 is 0.394 (compare with 0.516 for OH and O). Again, the outcome of the PBE0 calculation is similar, but the predicted correlation is even worse. The slope of the line is again far from the expected 0.5 with both functionals, and the deviation is particularly drastic in PBE0.

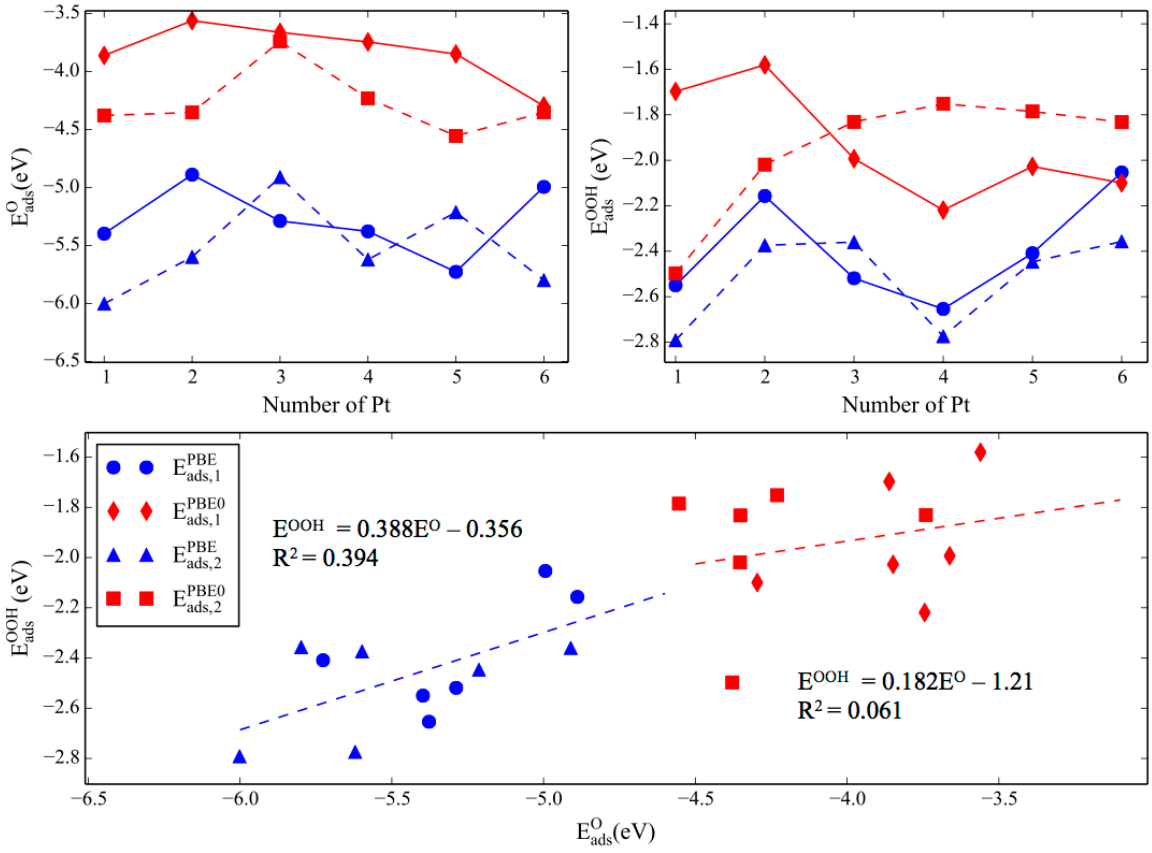

Figure 2. Scaling relationship between OOH and O binding energies. The blue and red data sets correspond to the PBE and PBE0 calculations, respectively. Color and style schemes, and data types are analogous to those used in Figure 1. Also, MAE for PBE data points is 0.15 eV and for PBE0 data points is 0.20 eV. MUE does not give a meaningful result due to the cancelation of error.

Figure 3 illustrates the scaling relationship between the OOH and OH binding energies. This particular correlation is the highest one obtained, with the R^2 value of 0.591. However, this value is still very low compared to that for metallic surfaces, which is usually in the range of 0.8–0.95. Furthermore, in this case, the slope of the line is 0.719, which deviates significantly from the expected value of 1.0, given that the O atom binding to the cluster has the same valency in OH and OOH. Interestingly, the binding energies of the first adsorbed OOH and OH correlate quite well across cluster sizes (Figure 3, upper panel, solid lines), leading to a stronger correlation. However, the effect of coverage is quite pronounced, and the binding energies for the second adsorbing OH and OOH exhibit very different trends (Figure 3, upper panel, dashed lines). These higher coverage results are responsible for the overall poor correlation (seen in Figure 3 bottom panel), and the failure of the scaling relationship. Coverage is not typically explored as a factor affecting scaling relations, but at least in the case of our clusters we see that it can be rather dramatic. The effect has to do with the cluster geometry change, and the change of the binding mode of OOH and OH when the second adsorbate binds, as discussed in detail below. Taken together, our findings so far suggest that small clusters can break the scaling relationship in catalysis, and exceed the intrinsic limit on catalytic activity.

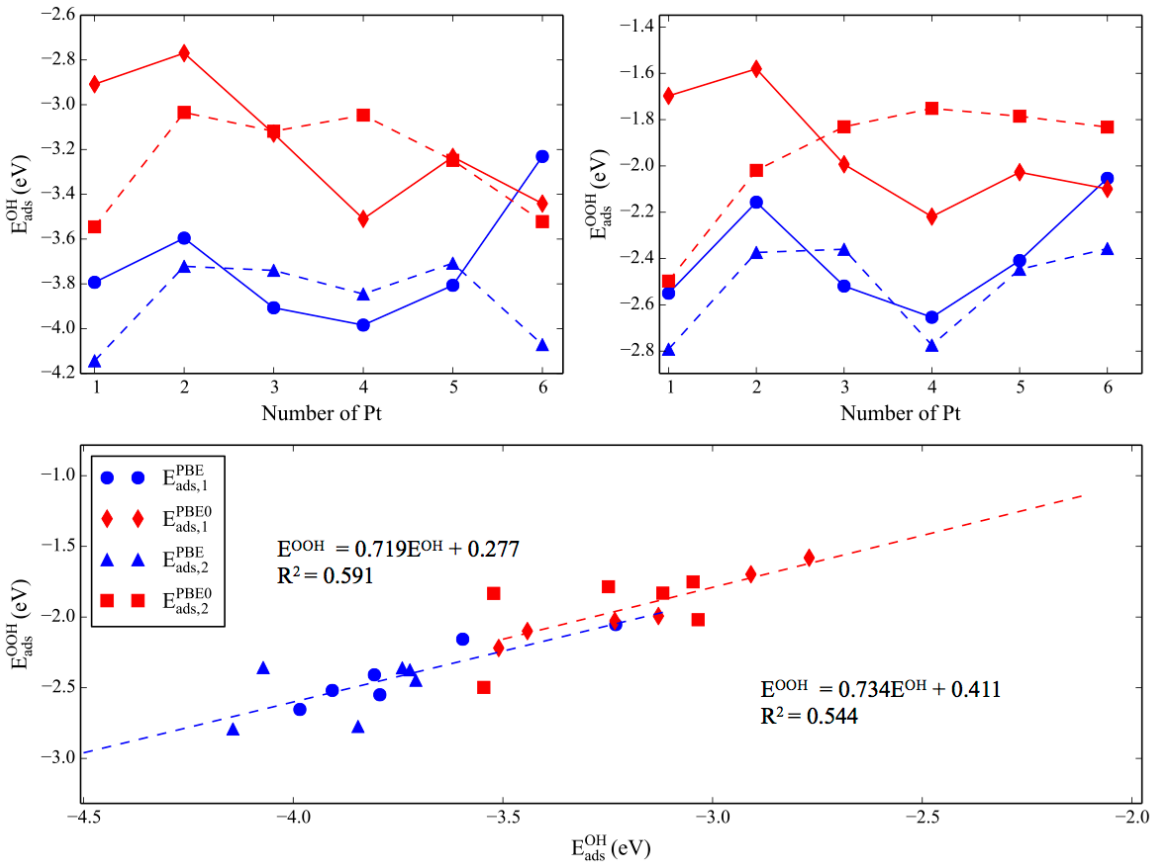

Figure 3. Scaling relationship between OOH and OH binding energies. Color and style schemes, and data types are analogous to those used in Figure 1. The data points corresponding to the second binding adsorbate in the lower panel are more scattered, being responsible for the overall poor correlation, regardless of the functional. Also, MAE for PBE data points is 0.10 eV and for PBE0 data points is 0.12 eV. MUE does not give a meaningful result due to the cancelation of error.

Figure 4 shows the global minimum structures of gas phase Pt clusters, before the adsorption, and upon binding the first and then the second adsorbate. These results were obtained with PBE0, and the corresponding PBE results are presented in the SI (Figures S1-S3). In general, the global minimum structure can be functional dependent. PBE functional gives a more flat structure for gas phase Pt_4, Pt_5, and Pt_6, whereas PBE0 predicts more globular geometries. However, these differences do not change the main conclusions of this study. Also, we have seen in the past that in thermal catalysis ensembles of many thermally-accessible catalyst states collectively determine catalyst properties, such as electronic characteristics,

Comparing the structures of Pt_nO, Pt_nOH, and Pt_nOOH (n=1–6) sheds light on their binding energies not showing a strong correlation. [40] activity,[41] selectivity,[42,43] and sintering resistance.[41–43] In the present case, temperatures are milder, and the thermal ensembles of clusters states are small, with the vast majority of the population occupying the global minimum by Boltzmann statistics. For all cases reported in this work, the adsorption energies calculated as ensemble averages minimally differ from the results calculated based on just the global minima. We present the ensemble data in the SI (Figures S4-S6), and focus on the global minima in the main text.

The change in cluster shape is adsorbate-dependent, suggesting that the cluster should be changing shape in the course of the catalyzed ORR reaction. For instance, $Pt_{5,6}$ change geometries when one of O, OH, or OOH binds, and the geometry is every time different. We have seen such behavior of small catalytic Pt clusters in the past,[40–44] and also found that cluster-shape change is exceptionally facile, allowing clusters visiting dozens on distinct minima in under 1 ns, even when on a supporting surface.[45] On the other hand, some clusters do not change shape so easily, such as Pt_4 and Pt_4O, Pt_4OH, and Pt_4OOH. In fact, the cluster size-dependence of the fluxionality adds to the unpredictability (poor correlation) of binding energies. The highly dynamic behavior, which is also size- and composition-dependent, is unique to subnano clusters, and certainly cannot be found in extended surfaces.

It is important to remark that in this work we operate under the assumption that the cluster has a chance to fully rearrange into an equilibrium thermodynamic ensemble in every minimum on the reaction profile. In other words, cluster dynamics is fast and decoupled from the reaction dynamics. This assumption is supported by our study of isomerization of Pt_7 on alumina, which appears to be exceptionally quick and structurally dramatic.[45] However, it is possible that this assumption is not generally applicable. Ideally, we would want to know how clusters isomerize, and which cluster isomers are really linked to each other in the reaction profile of ORR. This computational task would be exceptionally demanding, not within our reach.

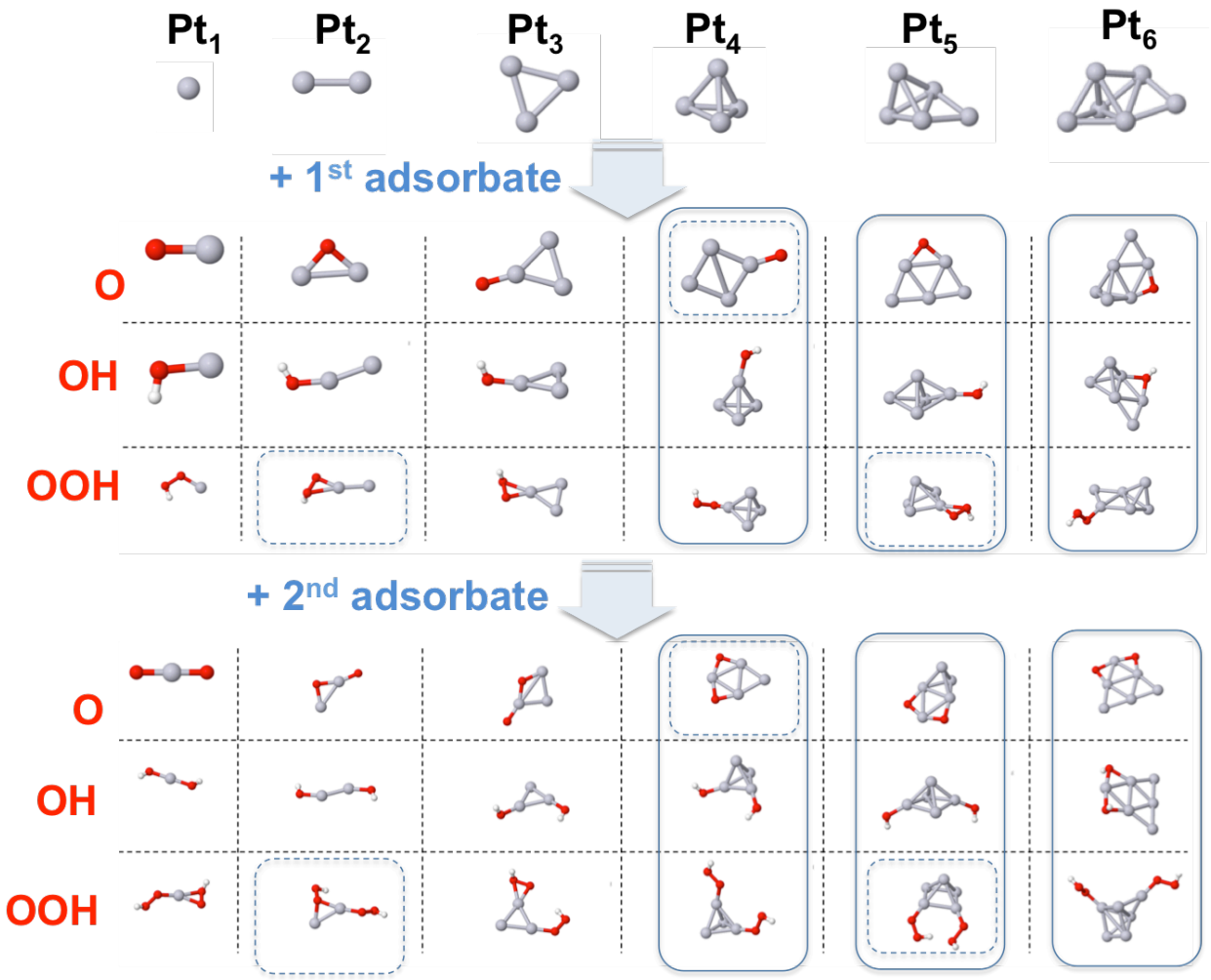

Figure 4. The global minimum structures of the gas phase Pt_n (n=1-6) clusters without bound adsorbates and with one and then two bound adsorbates, O, OH, and OOH. Clusters outlined with solid lines change shapes when going from adsorbate-free to adsorbate-bound, often changing also from one adsorbate to another. Clusters outlined in dashed lines change the binding site of the adsorbate when the coverage changes. Grey – Pt; red – O; white – H.

Secondly, the poor correlations between the binding energies of O, OH, and OOH can be traced to the additional effect of the binding site change. In scaling relationship, which was initially developed for extended surfaces, one usually assumes that the binding site does not change from surface to surface. However, as can be seen in Figure 4, binding sites can change from one cluster size to another. For example, O preferentially binds on atop site on Pt_4, but on a bridge site on Pt_5 and Pt_6. Also, OOH preferentially binds using both of its oxygen atoms when

on Pt_2, Pt_3, and Pt_6, but goes monodentate on atop position when on Pt_4 and Pt_5. In addition, O, OH, and OOH may preferentially bind to different sites on the same cluster. For example, O binds to the bridge site on Pt_5, whereas OH and OOH prefer atop site. For Pt_6, O and OH bind on a bridge, and OOH binds atop. These changes are fundamentally not too surprising, because every atom in such small clusters is unique in its coordination geometry and electronic structure. For example, a bridge site on Pt_4 is electronically not the same as that on Pt_5; every bridge site on every Pt_n is unique, etc.

When the coverage increases, the situation changes again (Figure 4). The second adsorbate may bind to the bridge site or atop, depending on the cluster. The binding position is often different from that of the first adsorbate, meaning that their chemistries are going to be different. For instance, in Pt_2O_2 and Pt_3O_2, and in $Pt_2(OOH)_2$, $Pt_3(OOH)_2$, and $Pt_5(OOH)_2$, the two adsorbates bind in two different sites, i.e. bridge and atop. Secondly, the second adsorbate can change the binding site of the first one. For instance, one O is bound atop on Pt_4, but, when two O atoms bind to Pt_4, both of them go on the bridge site. Similarly, OH bind to Pt_5 on a bridge, but two OH bind atop in $Pt_5(OH)_2$. It is clear that the change in the cluster shape and electronic structure after the binding of the first adsorbate, affects the binding site preference for the second adsorbate, and also the second adsorbate in turn changes the cluster and affects the binding of the first adsorbate. In a steady state in catalysis, clusters would be covered by different adsorbates at concentrations dictated by the conditions and the adsorption strengths, and so our model reveals only part of the story. However, it is clear that every time an adsorbate comes, goes, or changes in the reaction, the catalyst itself changes too, altering all other adsorption energies, and thus escaping the spell of the scaling relations.

In order to find out whether or not a similar behavior is characteristic of surface-deposited clusters, we choose to study at Pt_5 deposited on graphene, a support used as an electrode in ORR. Figure 5 shows the global minimum structures of Pt_5 on graphene, with and without the substrates, obtained via BH global optimization. Here too it can be seen that, when the adsorbate binds to the cluster, it changes its shape, particularly in PBE calculations (see SI) and particularly upon binding of the second adsorbate. The flat and upright shape of Pt_5 itself was seen also on MgO(100).[46] The second adsorbate can influence the preferred binding site for the first adsorbate. For instance, OH binds to the bridge site in Pt_5OH, but, as soon as the second OH binds, both adsorbates bind atop. Note the significant change in the structure of the cluster

after the second OH binds to it. In order to find out whether or not a similar behavior is characteristic of surface-deposited clusters, we choose to study at Pt_5 deposited on graphene, a support used as an electrode in ORR. Figure 5 shows the global minimum structures of Pt_5 on graphene, with and without the adsorbates, obtained from Basin Hopping algorithm.[47,48] Here too it can be seen that, when the adsorbate binds to the cluster, it changes its shape, particularly with PBE (see SI) and particularly upon binding of the second adsorbate. The flat and upright shape of Pt_5 itself was seen also on MgO(100).[46] The second adsorbate can influence the preferred binding site for the first adsorbate. For instance, OH binds to the bridge site in Pt_5OH, but, as soon as the second OH binds, both adsorbates bind atop. Note the significant change in the structure of the cluster after the second OH binds to it.

The computed binding energies for the surface-deposited cluster can be added to the trend lines shown in Figures 1-3. Doing this does not improve the trend and does not change the main conclusion (see Figures S7). The results suggest that small clusters, whether in the gas phase or on a supporting surface, would break scaling relations due to the changes in shape and in the adsorption binding sites, from one adsorbate to the next. We can also try to predict the adsorbate binding energies to the surface-deposited cluster from the trends obtained for the gas phase clusters (Figures 1-3), and compare the outcome to the calculations. Table 1 shows the comparison. It is important to emphasize that the trend line does not distinguish between the first and second binding energies. Therefore, it can be argued that the average error for OH binding energy is 0.07 eV, and for OOH it is 0.12 eV, i.e. a factor of 2 smaller than what is reported in Table 1. Overall, even though a single example is not enough for statistics, we see the error in the binding energies varies depending on the adsorbate and can be significant or negligible, in an unpredictable way.

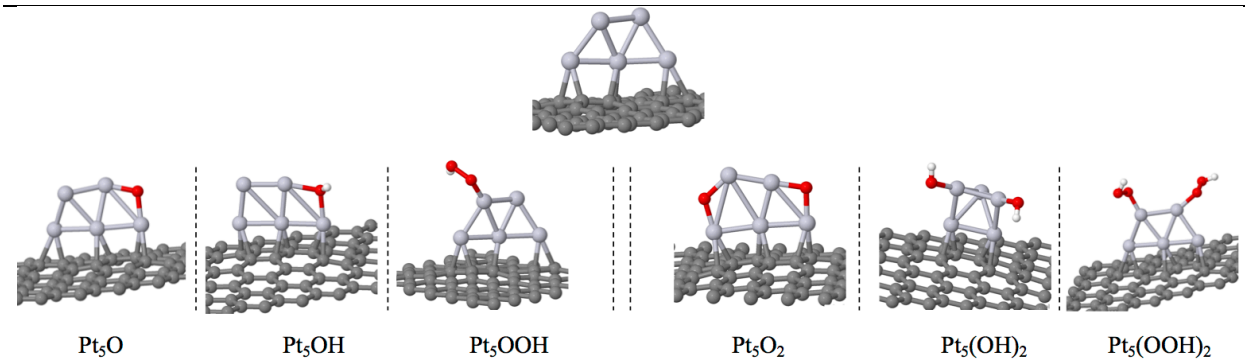

Figure 5. The global minimum structures for Pt_5 cluster deposited on graphene with different adsorbates and coverage obtained with PBE0.

. It is obvious, however, that using just one example does not show whether the trend line obtained from gas phase can be applied to the surface deposited clusters. In fact, Figure S7 shows that the slope of the line deviates even more from the expected value (0.5 for OH vs. O and 1.0 for OOH vs. OH) when the surface-supported results were added.

Table1. Comparison of calculated binding energies of different molecular intermediates on Pt_5 deposited on graphene with the predicted binding energies obtained from gas phase linear scaling relationships. All results obtained from PBE functional.

	$E^{O}_{ads,1}$(eV)	$E^{OH}_{ads,1}$(eV)	$E^{OOH}_{ads,1}$(eV)	$E^{O}_{ads,2}$(eV)	$E^{OH}_{ads,2}$(eV)	$E^{OOH}_{ads,2}$(eV)
Calculated	-5.36	-3.63	-2.23	-5.23	-3.77	-2.42
Predicted (from scaling)	-[a]	-3.77	-2.44	-[a]	-3.77	-2.44
Error	-	0.14	0.21	-	0.00	0.02

a. Reference state

In conclusion, because catalytic clusters at the subnano scale are exceptionally dynamic, and easily change shapes upon binding different adsorbates, they break scaling relations that otherwise impose constraints on the maximal achievable catalytic performance. Depending on the cluster size, the change of shape upon binding and changing adsorbates, and varying coverage may be greater or smaller. The binding sites of all adsorbates can be sensitive to the presence or absence of other adsorbates. As a result, correlations between the binding energies of adsorbates bound by scaling relations, such as O, OH, and OOH in ORR, become very lose, and their overall predictability becomes minimal. This is good news for catalysis, because it may

allow optimizing catalysis beyond the current limits for such precious processes as ORR and ammonia synthesis. The lever at cluster catalyst design that may enable this optimization are (i) cluster size (since dynamics is cluster size-specific), (ii) reagent concentrations (since the binding sites and correlations are affected by coverage), and (iii) to some degree, also temperature (since cluster dynamics is enabled by thermal effects). Nano-catalysts are yet again unusual as compared to extended surfaces, in this newly found way.

Computational methods: Plane wave density functional theory calculations were performed using Vienna Ab initio Simulation Package (VASP)[49–52] using projector augmented wave (PAW) potentials[53] and the PBE[54] functional. For the relaxation calculations presented in this paper, large kinetic energy cutoffs of 400.0 eV and convergence criteria of 10^{-6} eV were employed. Geometric relaxation was performed until forces on atoms were smaller than 0.01 eV/Å. Also, Gaussian smearing with the sigma value of 0.1 eV was used. Single point calculations were done using PBE0[55,56] functional on the structures obtained from the relaxation step using PBE functional. The energy cut-off of 0.8 eV was used in order to filter local minima structures obtained from PBE calculation, which are then fed into PBE0 single point calculation. Geometry relaxation of metal clusters using a hybrid functional, such as PBE0, usually causes some problem for the calculation to converge; however, geometries obtained from PBE calculations are usually reliable enough if a large enough energy cut-off is used to consider a significant number of local minima. A large unit cell of 20 Å × 20 Å × 20 Å was used for gas phase calculations. Note that, for gas phase calculations, in order to produce initial cluster geometries we used our in-house code, PGOPT,[3740] which automatically generates these structures based on the bond length distribution algorithm (BLDA).[37,38] Then each structure was optimized using DFT calculation, and duplicates were filtered out thereafter. For Pt_5 deposited on graphene, the Basin Hopping[47,48] algorithm implemented in PGOPT was used in order to find out the global and local minima structures. The experimental cell parameter of a = 2.46 Å was used for graphene.[57] The unit cell was grown to a (6 × 6) surface and a vacuum gap of 15 Å was used. This results in a supercell with parameters of a = 14.76 Å, b = 14.76 Å, c = 20.0 Å, α = 90°, β = 90°, and γ = 120°. Γ-point sampling was used for all calculations.

Acknowledgments

This work was supported by the Air Force Office of Scientific Research under a Basic Research Initiative grant (AFOSR FA9550-16-1-0141) and DOE-BES grant DE-SC0019152. CPU resources at the DOD (Department of Defense) High Performance Computing Modernization Program (the U.S. Air Force Research Laboratory DoD Supercomputing Resource Center–AFRL DSRC, the U.S. Army Engineer Research and Development Center–ERDC, and the Navy Supercomputing Resource Center–Navy DSRC), Pacific Northwest National Laboratory's Environmental Molecular Sciences Laboratory's (EMSL) Cascade cluster, Extreme Science and Engineering Discovery Environment's (XSEDE) computing resources, and the UCLA-IDRE cluster were used to conduct this work.

Supporting Information

Data obtained with PBE, scaling relations that include both gas phase and surface-deposited clusters, discussion on the performance of PBE versus PBE0.

All coordinate files (XYZ and POSCAR format) of Pt_5/graphene and gas phase Pt clusters along with the description of each file (README.md) can be found at the following address:

https://github.com/bzkarimi/scaling-Pt-ORR

References

(1) Montemore, M. M.; Medlin, J. W. Scaling Relations between Adsorption Energies for Computational Screening and Design of Catalysts. *Catal. Sci. Technol.* **2014**, *4*, 3748–3761.

(2) Greeley, J. Theoretical Heterogeneous Catalysis: Scaling Relationships and Computational Catalyst Design. *Annu. Rev. Chem. Biomol. Eng.* **2016**, *7*, 605–635.

(3) Liu, J. X.; Su, Y.; Filot, I. A. W.; Hensen, E. J. M. A Linear Scaling Relation for CO Oxidation on CeO2-Supported Pd. *J. Am. Chem. Soc.* **2018**, *140*, 4580–4587.

(4) Fernndez, E. M.; Moses, P. G.; Toftelund, A.; Hansen, H. A.; Martínez, J. I.; Abild-Pedersen, F.; Kleis, J.; Hinnemann, B.; Rossmeisl, J.; Bligaard, T.; et al. Scaling Relationships for Adsorption Energies on Transition Metal Oxide, Sulfide, and Nitride Surfaces. *Angew. Chemie - Int. Ed.* **2008**, *47*, 4683–4686.

(5) Busch, M.; Wodrich, M. D.; Corminboeuf, C. Linear Scaling Relationships and Volcano

Plots in Homogeneous Catalysis – Revisiting the Suzuki Reaction. *Chem. Sci.* **2015**, *6*, 6754–6761.

(6) Jiang, T.; Mowbray, D. J.; Dobrin, S.; Falsig, H.; Bligaard, T. Trends in CO Oxidation Rates for Metal Nanoparticles and Close-Packed, Stepped, and Kinked Surfaces. **2009**, *111*, 10548–10553.

(7) Fu, Q.; Cao, X.; Luo, Y. Identification of the Scaling Relations for Binary Noble-Metal Nanoparticles. *J. Phys. Chem. C* **2013**, *117*, 2849–2854.

(8) Calle-Vallejo, F.; Loffreda, D.; Koper, M. T. M.; Sautet, P. Introducing Structural Sensitivity into Adsorption-Energy Scaling Relations by Means of Coordination Numbers. *Nat. Chem.* **2015**, *7*, 403–410.

(9) Calle-Vallejo, F.; Tymoczko, J.; Colic, V.; Vu, Q. H.; Pohl, M. D.; Morgenstern, K.; Loffreda, D.; Sautet, P.; Schuhmann, W.; Bandarenka, A. S. Finding Optimal Surface Sites on Heterogeneous Catalysts by Counting Nearest Neighbors. *Science.* **2015**, *350*, 185–190.

(10) Quaino, P.; Juarez, F.; Santos, E.; Schmickler, W. Volcano Plots in Hydrogen Electrocatalysis-Uses and Abuses. *Beilstein J. Nanotechnol.* **2014**, *5*, 846–854.

(11) Sabatier, P. *La Catalyse En Chimie Organique*; Librarie Polytechnique, Paris, 1913.

(12) Gani, T. Z. H.; Kulik, H. J. Understanding and Breaking Scaling Relations in Single-Site Catalysis: Methane to Methanol Conversion by Fe^{IV}=O. *ACS Catal.* **2018**, *8*, 975–986.

(13) Khorshidi, A.; Violet, J.; Hashemi, J.; Peterson, A. A. How Strain Can Break the Scaling Relations of Catalysis. *Nat. Catal.* **2018**, *1*, 263–268.

(14) Calle-Vallejo, F.; Krabbe, A.; García-Lastra, J. M. How Covalence Breaks Adsorption-Energy Scaling Relations and Solvation Restores Them. *Chem. Sci.* **2016**, *8*, 124–130.

(15) Nilekar, A. U.; Mavrikakis, M. Improved Oxygen Reduction Reactivity of Platinum Monolayers on Transition Metal Surfaces. *Surf. Sci.* **2008**, *602*, 189–194.

(16) Shao, M.; Chang, Q.; Dodelet, J. P.; Chenitz, R. Recent Advances in Electrocatalysts for Oxygen Reduction Reaction. *Chem. Rev.* **2016**, *116*, 3594–3657.

(17) Tang, Z.; Wu, W.; Wang, K. Oxygen Reduction Reaction Catalyzed by Noble Metal Clusters. *Catalysts* **2018**, *8*, 1–18.

(18) Liu, M.; Zhang, R.; Chen, W. Graphene-Supported Nanoelectrocatalysts for Fuel Cells: Synthesis, Properties, and Applications. *Chem. Rev.* **2014**, *114*, 5117–5160.

(19) Wong, W. Y.; Daud, W. R. W.; Mohamad, A. B.; Loh, K. S. Effect of Temperature on the Oxygen Reduction Reaction Kinetic at Nitrogen-Doped Carbon Nanotubes for Fuel Cell Cathode. *Int. J. Hydrogen Energy* **2015**, *40*, 11444–11450.

(20) Tse, E. C. M.; Gewirth, A. A. Effect of Temperature and Pressure on the Kinetics of the Oxygen Reduction Reaction. *J. Phys. Chem. A* **2015**, *119*, 1246–1255.

(21) Okaya, K.; Yano, H.; Kakinuma, K.; Watanabe, M.; Uchida, H. Temperature Dependence of Oxygen Reduction Reaction Activity at Stabilized Pt Skin-PtCo Alloy/Graphitized Carbon Black Catalysts Prepared by a Modified Nanocapsule Method. *ACS Appl. Mater. Interfaces* **2012**, *4*, 6982–6991.

(22) Li, D.; Lv, H.; Kang, Y.; Markovic, N. M.; Stamenkovic, V. R. Progress in the Development of Oxygen Reduction Reaction Catalysts for Low-Temperature Fuel Cells. *Annu. Rev. Chem. Biomol. Eng.* **2016**, *7*, 509–532.

(23) Keith, J. A.; Jacob, T. Theoretical Studies of Potential-Dependent and Competing Mechanisms of the Electrocatalytic Oxygen Reduction Reaction on Pt(111). *Angew. Chemie - Int. Ed.* **2010**, *49*, 9521–9525.

(24) Chen, J.; Eguchi, K.; Waki, K. The Effect of Oxidation Temperature for the Oxygen Reduction Reaction Activity of Defective Multi-Walled Carbon Nanotubes (MWCNT). *ECS Trans.* **2017**, *80*, 677–684.

(25) Guo, S.; Zhang, S.; Sun, S. Tuning Nanoparticle Catalysis for the Oxygen Reduction Reaction. *Angew. Chemie - Int. Ed.* **2013**, *52*, 8526–8544.

(26) Wu, J.; Yang, H. Platinum-Based Oxygen Reduction Electrocatalysts. *Acc. Chem. Res.* **2013**, *46*, 1848–1857.

(27) Huang, X.; Cao, L.; Chen, Y.; Zhu, E.; Lin, Z.; Li, M.; Yan, A.; Zettl, A.; Wang, Y. M.; Duan, X.; et al. High-Performance Transition Metal-Doped Pt3Ni Octahedra for Oxygen Reduction Reaction. *Science.* **2015**, *348*, 1230–1234.

(28) Bu, L.; Zhang, N.; Guo, S.; Zhang, X.; Li, J.; Yao, J.; Wu, T.; Lu, G.; Ma, J. Y.; Su, D. Biaxially Strained PtPb/Pt Core/Shell Nanoplate Boosts Oxygen Reduction Catalysis. *Science.* **2016**, *354*, 1410.

(29) Shao, M.; Peles, A.; Shoemaker, K. Electrocatalysis on Platinum Nanoparticles: Particle Size Effect on Oxygen Reduction Reaction Activity. *Nano Lett.* **2011**, *11*, 3714–3719.

(30) Imaoka, T.; Kitazawa, H.; Chun, W. J.; Yamamoto, K. Finding the Most Catalytically

Active Platinum Clusters with Low Atomicity. *Angew. Chemie - Int. Ed.* **2015**, *54*, 9810–9815.

(31) Imaoka, T.; Kitazawa, H.; Chun, W. J.; Omura, S.; Albrecht, K.; Yamamoto, K. Magic Number Pt_{13} and Misshapen Pt12clusters: Which One Is the Better Catalyst? *J. Am. Chem. Soc.* **2013**, *135*, 13089–13095.

(32) Yamamoto, K.; Imaoka, T.; Chun, W. J.; Enoki, O.; Katoh, H.; Takenaga, M.; Sonoi, A. Size-Specific Catalytic Activity of Platinum Clusters Enhances Oxygen Reduction Reactions. *Nat. Chem.* **2009**, *1*, 397–402.

(33) Miyazaki, K.; Mori, H. Origin of High Oxygen Reduction Reaction Activity of Pt_{12} and Strategy to Obtain Better Catalyst Using Sub-Nanosized Pt-Alloy Clusters. *Sci. Rep.* **2017**, *7*, 45381.

(34) Nigam, S.; Majumder, C. ORR Viability of Alumina-Supported Platinum Nanocluster: Exploring Oxidation Behaviour by DFT. *Phys. Chem. Chem. Phys.* **2017**, *19*, 19308–19315.

(35) Lim, D. H.; Wilcox, J. Mechanisms of the Oxygen Reduction Reaction on Defective Graphene-Supported Pt Nanoparticles from First-Principles. *J. Phys. Chem. C* **2012**, *116*, 3653–3660.

(36) Wang, W.; Lei, B.; Guo, S. Engineering Multimetallic Nanocrystals for Highly Efficient Oxygen Reduction Catalysts. *Adv. Energy Mater.* **2016**, *6*, 1–16.

(37) Pickard, C. J.; Needs, R. J. Ab Initio Random Structure Searching. *J. Phy. Condens. Matter* **2011**, *23*, 053201–053223.

(38) Pickard, C. J.; Needs, R. J. Structures at High Pressure from Random Searching. *Phys. Status Solidi Basic Res.* **2009**, *246*, 536–540.

(39) Demiroglu, I.; Yao, K.; Hussein, H. A.; Johnston, R. L. DFT Global Optimization of Gas-Phase Subnanometer Ru-Pt Clusters. *J. Phys. Chem. C* **2017**, *121*, 10773–10780.

(40) Zhai, H.; Alexandrova, A. N. Ensemble-Average Representation of Pt Clusters in Conditions of Catalysis Accessed through GPU Accelerated Deep Neural Network Fitting Global Optimization. *J. Chem. Theory Comput.* **2016**, *12*, 6213–6226.

(41) Baxter, E. T.; Ha, M. A.; Cass, A. C.; Alexandrova, A. N.; Anderson, S. L. Ethylene Dehydrogenation on $Pt_{4,7,8}$ Clusters on Al_2O_3: Strong Cluster Size Dependence Linked to Preferred Catalyst Morphologies. *ACS Catal.* **2017**, *7*, 3322–3335.

(42) Ha, M. A.; Baxter, E. T.; Cass, A. C.; Anderson, S. L.; Alexandrova, A. N. Boron Switch for Selectivity of Catalytic Dehydrogenation on Size-Selected Pt Clusters on Al_2O_3. *J. Am. Chem. Soc.* **2017**, *139*, 11568–11575.

(43) Jimenez-Izal, E.; Zhai, H.; Liu, J. Y.; Alexandrova, A. N. Nanoalloying MgO-Deposited Pt Clusters with Si to Control the Selectivity of Alkane Dehydrogenation. *ACS Catal.* **2018**, *8*, 8346–8356.

(44) Zhai, H.; Alexandrova, A. N. Fluxionality of Catalytic Clusters: When It Matters and How to Address It. *ACS Catal.* **2017**, *7*, 1905–1911.

(45) Zhai, H.; Alexandrova, A. N. Local Fluxionality of Surface-Deposited Cluster Catalysts: The Case of Pt_7 on Al_2O_3. *J. Phys. Chem. Lett.* **2018**, *9*, 1696–1702.

(46) Shen, L.; Dadras, J.; Alexandrova, A. N. Pure and Zn-Doped Pt Clusters Go Flat and Upright on MgO(100). *Phys. Chem. Chem. Phys.* **2014**, *16*, 26436–26442.

(47) Oganov, A. R. *Modern Methods of Crystal Structure Prediction*; Wiley-VCH Verlag GmbH & Co. KGaA: Weinheim, Germany, 2010.

(48) Zhai, H. J.; Zhao, Y. F.; Li, W. L.; Chen, Q.; Bai, H.; Hu, H. S.; Piazza, Z. A.; Tian, W. J.; Lu, H. G.; Wu, Y. B.; et al. Observation of an All-Boron Fullerene. *Nat. Chem.* **2014**, *6*, 727–731.

(49) Kresse, G.; Furthmiiller, J. Efficiency of Ab-Initio Total Energy Calculations for Metals and Semiconductors Using a Plane-Wave Basis Set. *Comput. Mater. Sci.* **1996**, *6*, 15–50.

(50) Kresse, G.; Hafner, J. Ab Initio Molecular Dynamics for Liquid Metals. *Phys. Rev. B* **1993**, *47*, 558–561.

(51) Kresse, G.; Furthmüller, J. Ab Initio Molecular-Dynamics Simulation of the Liquid-Metal-Amorphous-Semiconductor Transition in Germanium. *Phys. Rev. B* **1994**, *40*, 14251–14271.

(52) Kresse, G.; Furthmüller, J. Efficient Iterative Schemes for Ab Initio Total-Energy Calculations Using a Plane-Wave Basis Set. *Phys. Rev. B* **1996**, *54*, 11169–11186.

(53) Kresse, G.; Joubert, D. From Ultrasoft Pseudopotentials to the Projector Augmented-Wave Method G. *Phys. Rev. B* **1999**, *59*, 1758–1775.

(54) Perdew, J. P.; Burke, K.; Ernzerhof, M. Generalized Gradient Approximation Made Simple. *Phys. Rev. Lett.* **1996**, *77*, 3865–3868.

(55) Perdew, J. P.; Ernzerhof, M.; Burke, K. Rationale for Mixing Exact Exchange with

Density Functional Approximations. *J. Chem. Phys.* **1996**, *105*, 9982–9985.

(56) Adamo, C.; Barone, V. Toward Reliable Density Functional Methods without Adjustable Parameters: The PBE0 Model. *J. Chem. Phys.* **1999**, *110*, 6158–6170.

(57) Reddy, D.; Register, L. F.; Carpenter, G. D.; Banerjee, S. K. Graphene Field-Effect Transistors. *J. Phys. D. Appl. Phys.* **2011**, *44*, 313001–313020.

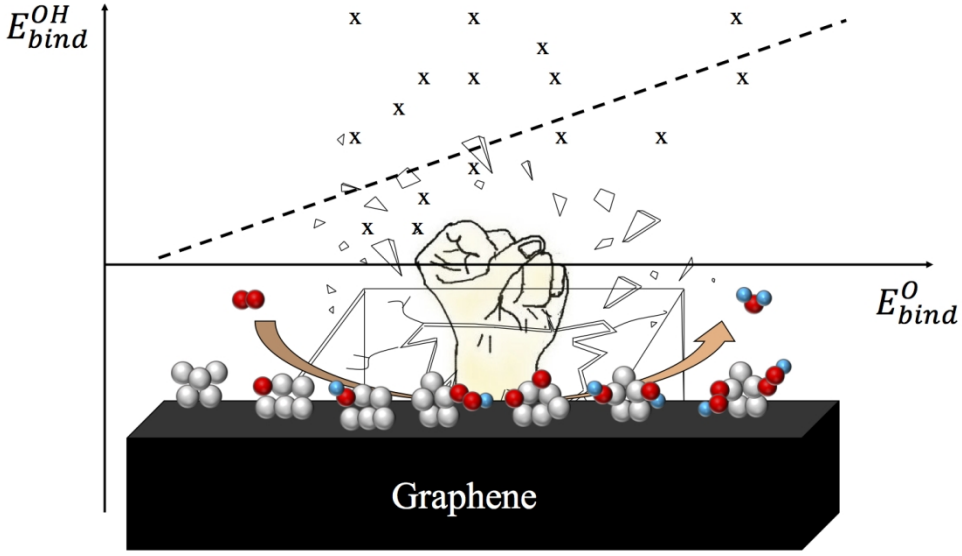

TOC graphics

338x190mm (120 x 120 DPI)

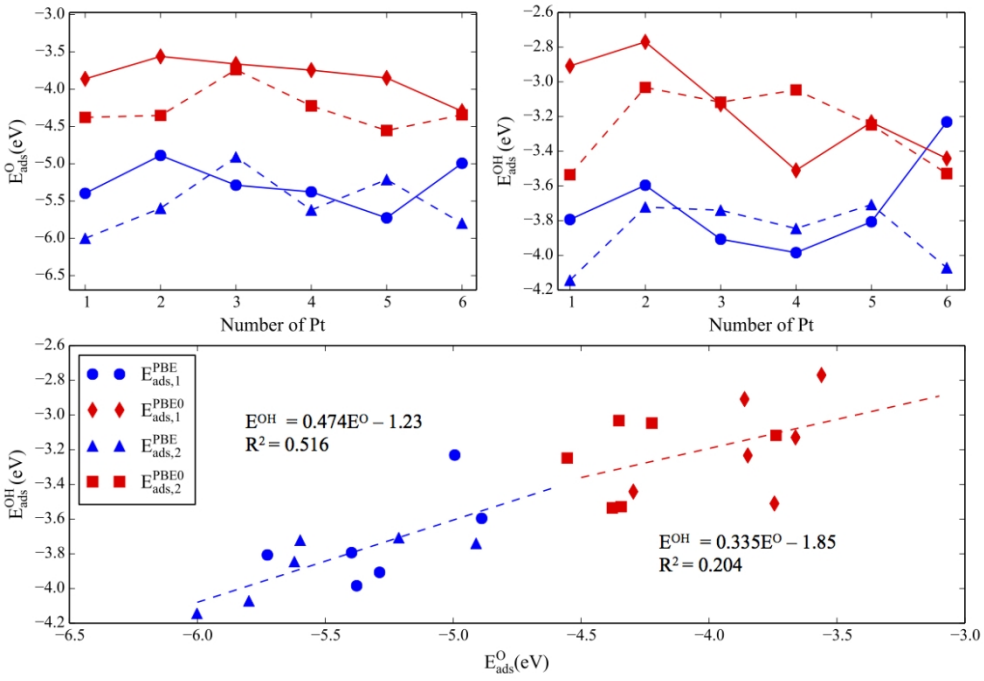

Figure 1

249x174mm (120 x 120 DPI)

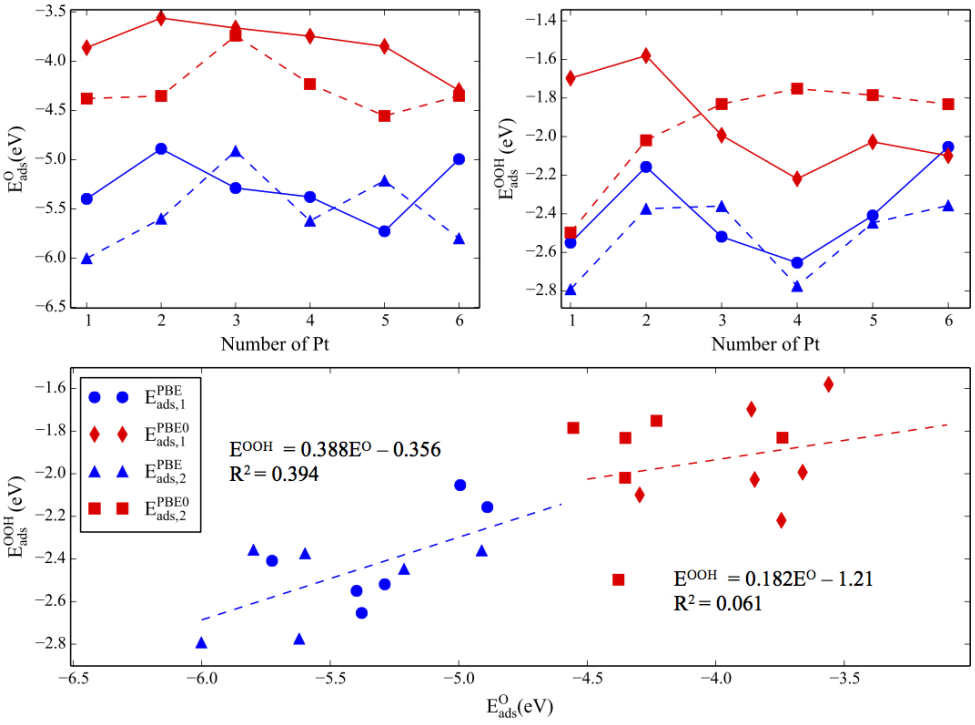

Figure 2

232x174mm (120 x 120 DPI)

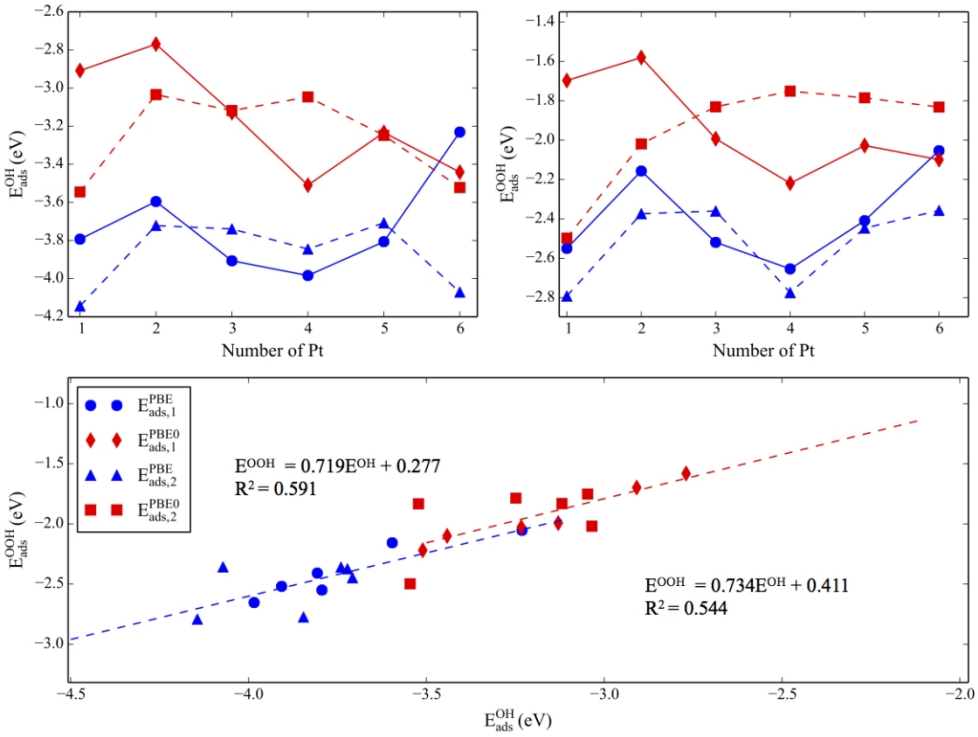

Figure 3

252x187mm (120 x 120 DPI)

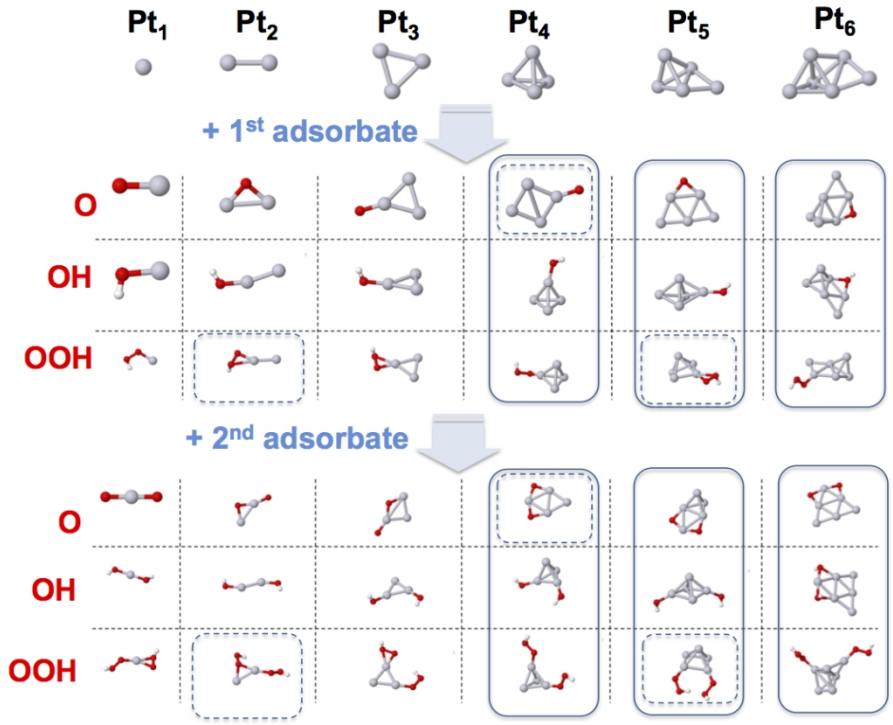

Figure 4

254x190mm (120 x 120 DPI)

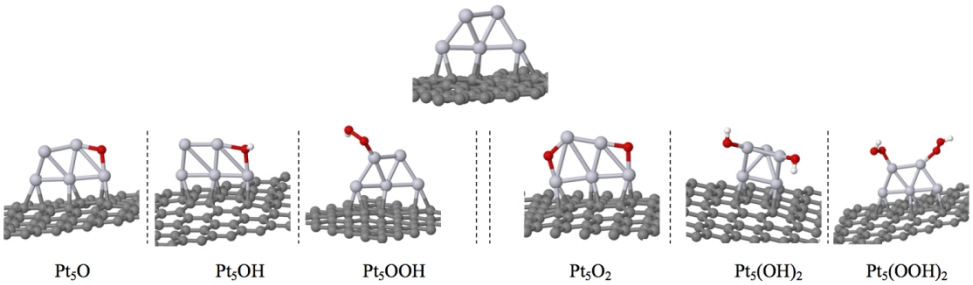

Figure 5

337x112mm (120 x 120 DPI)